Chapter 5: Multimodal Imaging of Gadolinium Oxide nanoclusters

5.1 Introduction

A multimodal imaging probe, which combines many imaging modalities in a synergistic manner, has been shown to be a potent tool for early disease detection and treatment with high precision and accuracy. [205,431,432] Because of its high spatial and subcellular resolution, deep tissue penetration, and sensitivity, the fluorescence (FL) /magnetic resonance (MR) imaging probe attracts significant attention in biomedical research and is successfully implemented in clinical practice. [286,433] There has been much interest in developing safer and more efficient nanoscale dual-modal imaging probes (FL/MR) with tunable physicochemical properties and good biodistribution. [240,284] Recently, Gd_2O_3 nanomaterials have gained huge scientific attention due to their capacity to enhance and improve imaging modalities such as Magnetic Resonance Imaging (MRI). [196] Gd-based contrast agents are particularly appealing because of gadolinium's large magnetic moment (7 unpaired electrons) and suitability towards multiple organs such as the liver, spleen, and lungs. [227,434] Gd_2O_3 nanomaterials are favoured among other Gd-based contrast agents because of their larger molecular weight (prevents rapid renal elimination) and great r_1 relaxivity. [202,206,435] The relaxation time (T_1) largely depends on the surface functionalization, compositions, and size of the contrast agent. In previous reports, it has been demonstrated that the ideal size of Gd_2O_3 NPs for maximal contrast enhancement would lie between 1–2.5 nm. [228,262,278] Although contrast-enhanced MRI is well known for its great spatial resolution, it suffers from low intensity. Multimodal imaging is helpful in this sense. The goal of multimodal imaging is to compensate for the shortcomings of one imaging modality with the strengths of the others. [202,283] The low intensity of MRI can be supplemented with high-intensity fluorescence Imaging (FI) or optical imaging. Gd_2O_3

nanomaterials functionalize with luminescent material and can be employed as a contrast agent in MRI as well as fluorophores in fluorescence imaging. Although Gd does not exhibit visible luminescence (due to its high singlet and triplet energies), it can produce luminescence through heavy atom impact. [202] The heavy atom of gadolinium influences the mixing of singlet and triplet states in its surroundings, which results in better quantum efficiency or luminescence intensity. Despite having widespread interest in the use of Gd_2O_3 nanomaterials, existing synthesis techniques are complex, require high reaction temperatures (≥ 180 °C), and are time-consuming. [223,289] Polyol synthesis method dominantly use for the preparation of gadolinium oxide NPs but low crystallinity and generation of organic by-products affect the particles' biological interaction and optical properties, limiting their biological application. [204] The popular synthesis technique described in article of Bazzi R et al. [436] and its modifications, in particular, require heating the precursor's solution for 1 hr. at 140 °C and then for another 4 hrs. at 180 °C. Furthermore, F.Goubard et.al discussed that any change in solvent like diethylene glycol (DEG) to water ratio, heating duration, or temperature can cause considerable particle size fluctuations. Except for the solvent, no additional nanoparticle stabilization method is offered in these techniques. Except for the final step, in which the authors use several organic acids, including CA, for NP functionalization, the synthesis processes described by Soderlind et al. [437] are nearly identical to those described in research article by R.Bazzi et al. Particle size distributions in the 5-15 nm range can be achieved using these approaches. [437] A alternative approach in which trioctylphosphine oxide is utilized as a capping agent, yields particle size distributions in the 40-60 nm range. [437] Park et al. devised a novel synthesis process that uses synthesis temperatures as high as 260 °C and times as long as 1 day. [438] From the foregoing, it is clear that there is a definite need for the development of a more convenient approach for the synthesis of Gd_2O_3 nanoparticles

in the target size range of 1-2.5 nm, as proposed in by Ja Young Park et al. The goal of the current work is to develop a simpler synthesis route with a shorter preparation time and lower synthesis temperature compared to the reported methods to synthesize optimal Gd_2O_3 nanoclusters with the size regime necessary for maximal contrast enhancement in MRI. In addition, we aim to use a capping agent that simultaneously suppresses nanoparticle agglomeration efficiently and shows luminescence in the visible region. In this regard, chitosan appears to be the nanoparticle stabilizer of choice. [439–441] We anticipate that carrying out synthesis in the presence of chitosan and ascorbic acid would reduce particle size.

5.2. Experimental section

5.2.1 Chemicals used

99.9% pure gadolinium (III) nitrate hexahydrate was obtained from Sigma Aldrich. SRL Private Limited was contracted to acquire superior quality medium molecular weight chitosan and sodium hydroxide granules (NaOH) and L-Ascorbic acid was purchased from Sigma Aldrich. Throughout the reaction, ultrapure deionized water was utilized, and all of the listed compounds were utilized without further adulteration or purification.

5.2.2 Synthesis procedure

Before carrying out the reaction, every glassware was cleansed with aqua regia. Briefly, gadolinium (III) nitrate hexahydrate salt (5 mM,10 ml) and chitosan (25 mg/ml, 5 ml) were dissolved in deionized water and stirred for 5 minutes at 55 ^{o}C. Consequently, 1 mL of 1M NaOH was added dropwise to maintain a pH near to 10. Following the addition of 20 mg/ml L-ascorbic acid, the resulting solution was agitated for 2 hrs. at 55 ^{o}C before being incubated for 24 hrs. Throughout the duration of the reaction, the flask was securely sealed

with cotton plugs and parafilm. The color of the solution transformed from colorless to pale yellow after 72 hrs. of incubation. The yellow solution was centrifuged for 5 minutes at 15k rpm to remove larger particles and unreacted ligands. For all feasible controls, the same synthesis procedure was utilized.

5.2.3 Characterization

Size analysis using an FEI Tecnai G2 20 TWIN transmission electron microscope (TEM) with an accelerating voltage of 200 kV. The 10-fold diluted sample was drop-cast onto a carbon-coated copper grid and allowed to air-dry at ambient temperature. The PTI Quanta master 400 (Slit width = 1 nm, integration time = 0.1s, and step size = 1 nm) and the Elico SL210 spectrophotometer were used to record the fluorescence and UV-Vis absorbance spectra, respectively. Fourier transforms infrared (FTIR) spectroscopy was acquired with a Nicolet iS5, THERMO Electron Scientific Instruments LLC instrument in the range of 400-4000 cm^{-1}. The instruments used for X-ray diffraction (XRD) and X-ray photoelectron spectroscopy (XPS) were the Rigaku Miniflex 600 Desktop X-Ray Diffraction System (RIGAKU Corporation) and the K-Alpha (Thermo Fisher Scientific). The SP8 STED model of the Leica microsystem was utilized for imaging investigations of brain cells. Quantum yield calculations were performed on Horiba PTI Fluorescence Quanta Master 400 Systems, and absolute quantum yields (QYs) of the synthesized nanoparticles were determined with a PTI K - Sphere diminutive Integrating sphere. In vivo fluorescence imaging system (IVIS imaging) (Photon Optima Imager, manufactured, Biospace, France) used to collect fluorescence signals.

5.2.4 Cytotoxicity estimation

The cytotoxicity of human brain cells treated with Gd_2O_3 nanoclusters was evaluated utilizing a colorimetric assay based on the reaction between yellow tetrazolium salt MTT (3-(4, 5-dimethylthiazol-2-yl)-2, 5-diphenyl tetrazolium bromide) and the mitochondrial succinate dehydrogenase of living cells, yielding purple-colored formazan crystals. The cell line was grown at 37 ºC in a humidified 5% CO_2 atmosphere in high glucose complete DMEM (10% FBS, 20 mM L-glutamine, 100 units/mL penicillin, and 100 g/mL streptomycin). In order to evaluate adhesion, 1×10^6 U-87 MG cells were seeded into each well of two separate 96-well plates and incubated for 24 hrs. After 24 hrs. of incubation at 37 ºC in a 5% CO_2 humidified atmosphere, the initial medium was discarded and substituted with fresh DMEM containing various concentrations of different nanoparticles (0.1, 0.01, and 0.001 concentrations of 5.9 mg/ml stock solution). After withdrawing the media from each well, a 5 mg/mL MTT solution in 100 L of fresh medium was added, and the plates were incubated for an additional two hrs. After 30 minutes of incubation at 37 ºC in the dark, the MTT solution was discarded, and 100 mL of DMSO was added to each well to dissolve the formazan crystal. Micro ELISA plate scanners set to 570 nm measured the intensity of the generated color. This formula was used to estimate the approximate viability of cells:

% Cell viability = [O.D of Gd_2O_3 nanoclusters treated cells / O. D of Control cells] ×100

5.2.5 Hemocompatibility assay

Through haemolysis, the safety of Gd_2O_3 nanoclusters towards the blood of healthy subjects was evaluated. After centrifugation, the red blood cells in the detritus were washed with PBS. In an eppendorf microtube, 0.2 ml of washed blood and 0.8 ml of Gd_2O_3 nanoclusters (diluted in saline) were combined for 2 hrs. followed by 30 minutes with

moderate stirring. After incubation, the samples were centrifuged at 2k rpm for 10 minutes. The supernatant was then dispensed at a volume of 100 µl into the 96-well plate. The absorbance was measured at 570 nm, which is deemed the wavelength of maximum absorption. Positive control consisted of distilled water, while negative control was PBS. The percentage of hemolysis was calculated using the following formula:

$$\textbf{\% Hemolysis} = [(\text{Abs T} - \text{Abs C})/(\text{Abs100\%} - \text{Abs C})\text{X100}]$$

AbsT is the absorbance of the supernatant of the particles-incubated samples, AbsC is the absorbance of the negative control supernatant (PBS), and Abs100% is the absorbance of the positive control supernatant.

5.2.6 Histopathology in rat

Healthy rats of both genders ranging 200-250 g weight were collected and kept in natural environments with a temperature of 25± 2 °C and a relative humidity of 50-60%. They were given full-price nutritional pellet feed and sterile water ad libitum for 4-5 days before the studies began. After one week of acclimatization, nine Charles Foster (CF) rats weighing 250± 20 grams were randomly allocated into two groups (n = 6). Group 1 received a conventional saline intravenous injection through the lateral tail vein, while Group 2 received a Gd_2O_3 NCs injection. Histopathology studies were conducted on vital organs such as the brain, lungs, liver, kidneys, and spleen of the rats. The rats were treated with saline (control) and Gd_2O_3 NCs (dosed at 70 mg/kg) and were euthanized at three different time points: 3 hrs., 7 days, and 28 days post-treatment. Three rats were euthanized at each time point, and their organs were collected for histopathological analysis. The collected organs were washed with a saline solution, fixed in a 10% formalin solution, and embedded in paraffin. Paraffin sections of 5 µm thickness were then cut and mounted on

glass slides. After staining with haematoxylin and eosin (HE) for cytoplasmic contrast, the sections were examined under a light microscope to observe any histopathological changes.

5.2.7 Clinical signs and body weight measurement

Rats (250 ± 20 g) were randomly divided into two groups (n=6). The first group will be given normal saline (control group), whereas the second group will be given Gd_2O_3 NCs dissolved in saline. Before and 0-3 hrs. after administration of the Gd_2O_3 NCs, animal appearance, activity, hair, probable trauma, faeces, and mortality were observed. Weight change, an essential toxicity index for rats, was assessed before and after dosing with 0.5 ml of Gd_2O_3 NCs on the second, seventh, and 28th days. There were no obvious changes observed between the dosage groups and the control.

5.2.8 In vivo biodistribution and fluorescence signal in the healthy Rat after Gd_2O_3 NCs administration

The aim was to investigate the biodistribution and live fluorescence signals of Gd_2O_3 NCs administrated Swiss albino mice. In this study, 500 µL (5.9 mg/ml stock) Gd_2O_3 NCs solution was injected through the tail vein of healthy mice. The fluorescence signal in the mice was observed at different time intervals after Gd_2O_3 NCs dosing. On the contrary, the control group mice did not receive any intravenous injections. The data obtained from the study was analysed using M3Vision software to draw conclusions and insights

5.2.9 Absolute Quantum yield

The sample and blank (DI water) filled 1 cm 4 side transparent quartz cuvette was mounted in the center of the integrating sphere to maximize the interaction of incident light with the sample in order to compute the absolute quantum yield of Gd_2O_3 NCs (absorbance value ~ 0.1) at blue green region (4.4 % and 7.1 % respectively). The integrating sphere catches all

of the light that a fluorescent sample emits and disperses. Various excitations were applied to samples using an A-1010 B 75 W Xe PTI arc lamp housing. The accuracy of the spectral correction was determined by comparing the corrected emission spectra of a standard dye, Rhodamine 6G (in ethanol = 0.95), computed with the integrating sphere configuration to the corresponding spectra acquired with a calibrated spectrofluorometer. [442]

5.2.10 Relaxivity measurement

In 2 ml Eppendorf tube containing milli-Q water, a series of aqueous solutions of Gd_2O_3 NCs samples with varied Gd concentrations (0.2, 0.3, 0.4, 0.5, 1.0, and 1.5 mM) were created for *in-vitro* MR research. A Philips 3 Tesla Multi Transmit 32/48 Channel MRI System instrument with a head coil was used to assess longitudinal relaxation times (T1) for the images of Gd_2O_3 NCs samples. T1-weighted MR imaging was performed using an inverse recovery pulse sequence (T1W_IR_TSE) with the following parameters: The field of view (FOV) was 25 cm, the matrix size was 256 × 404, the slice thickness was 4 mm with the spacing gap of 0, and the time to echo (TE) was 20 ms, repetition time (TR) was 2000 ms and the Inversion time (TI) was adjusted from 100 - 4000 ms. The *Philips DICOM Viewer R3.0-SP* 15 software was used to acquire net MRI single amplitude data at each concentration using the signal intensity of the appropriate region of interest (RIO) recorded at each TI (Inversion Time). This MRI signal data was used to calculate T1 (longitudinal relaxation time) using a non-linear least-square regression using the equation 1: -

$$M_z = Mo\left(1 - exp^{-t/T_1}\right) \dots\dots\dots\dots\dots\dots 1$$

Where Mz z-axis of Magnetization, which is the selected area magnetization at each inversion time (TI). Fitted parameters T_1 and M_0 are MRI signals amplitude at TI =0 and the sample's concentration-dependent relaxation time was determined simultaneously for

each concentration. Now, the r_1 relativities of each sample were determined by the slopes of the plots of relaxation rates $1/T_1$ against Gd concentration, respectively. [234,235,262]

5.3 Result and discussion

Gd_2O_3 NCs was prepared using a facile one-pot technique using chitosan and ascorbic acid as stabilizing and reducing agent, respectively. Color transformation after a 2 hrs. reaction, from colorless to light yellow, indicates the initiation of nucleation and new phase development; after 72 hrs. incubation, the pale-yellow color visually confirmed the origin of the stable new phase, i.e., Gd_2O_3 NCs. Furthermore, to characterize the nanoclusters, several microscopic and spectroscopic techniques were acquired, which confirmed the size, shape, composition, and phase of Gd_2O_3 NCs.

5.3.1 Fluorescence spectroscopy and UV–Vis spectroscopic characterization

Fluorescence spectra of Gd_2O_3 NCs and all possible controls were acquired using a fluorescence spectrofluorometer. The aqueous suspension of Gd_2O_3 NCs exhibited sharp emission spectra at 447 nm (blue), 535 nm (green), and 605 nm (red) at excitation wavelengths of 365, 465, and 550 nm, respectively (Figure 5.1). These spectra are symbolic of the successful origin of fluorescence species (Gd_2O_3 NCs). To explicit the fluorescence origin, all possible controls were taken and analysed their fluorescence behaviour. From the control emission spectra, we observed negligible fluorescence in the red and green channels, whereas emission in blue is observed, but compared to Gd_2O_3 NCs, it is very less and insignificant to stain cells hence, we conclude that the presence of both chitosan and ascorbic acid is crucial for the generation of fluorescent Gd_2O_3 NCs. [443–446] The UV−vis absorbance spectra of Gd_2O_3 NCs did not show any peak in the region 400−800 nm (Figure 5.1 (d)), thus excluding the development of large-size SPR active Gd_2O_3 NCs.

However, the spectrum consisted of sharp peaks at 273 nm; the origin of this is attributed to the formation of gadolinium-thiolate complexes, either as independent species or on the surface of clusters of Gd_2O_3 atoms. Additionally, the spectrum of pure chitosan displayed no peak in the region. The disappearance of the peak at 300-400 nm following the reaction, accompanied by the absence of the SPR peak, indicated possible conversion of the Gd salt into Gd_2O_3 NCs. [232,444,447]

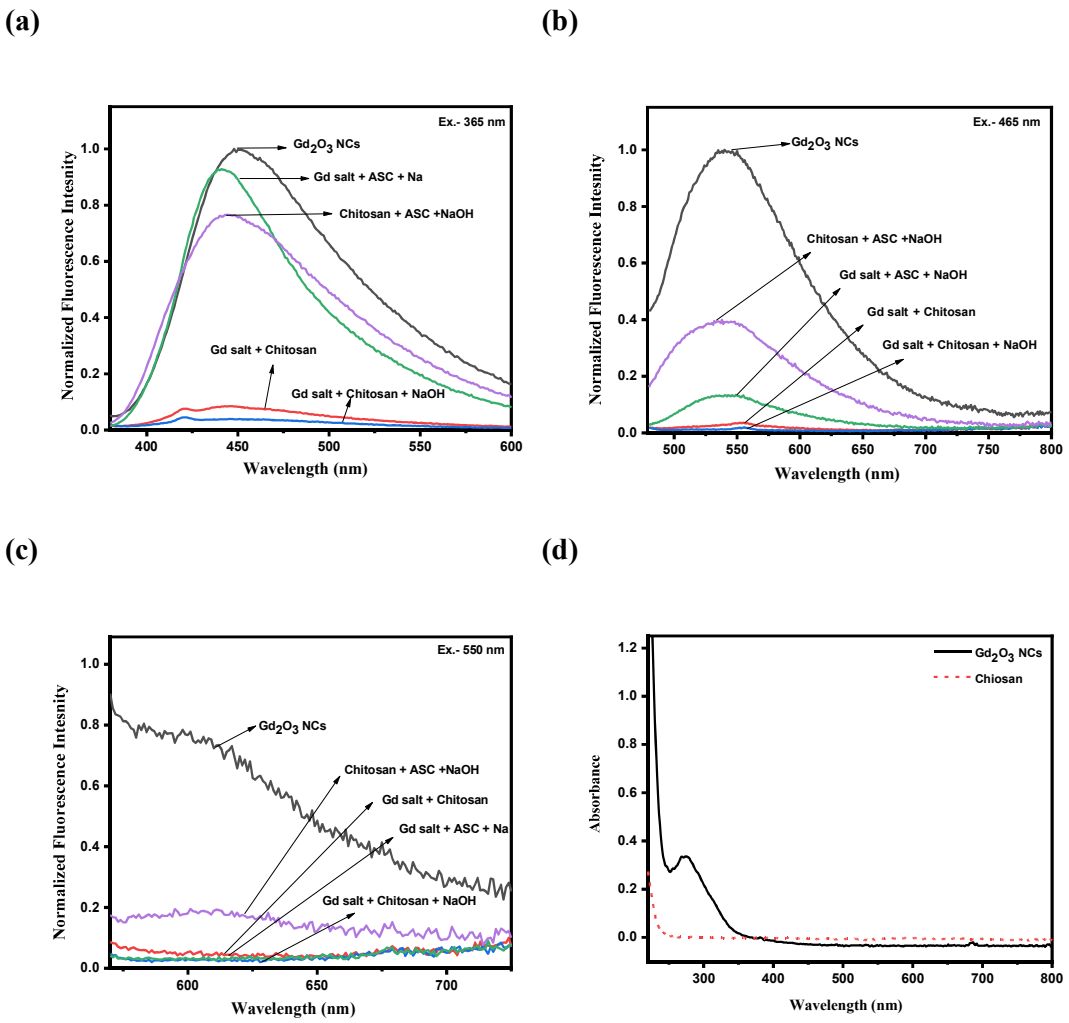

Figure 5.1: The fluorescence emission spectra of Gd_2O_3 NCs and all possible controls. (a) The normalized emission spectra of Gd_2O_3 NCs and control at Ex- 365 / Em- 447, (b) The normalized emission spectra of Gd_2O_3 NCs and control at Ex- 465 / Em- 535 (c) The normalized emission spectra of Gd_2O_3 NCs and control at Ex- 550 / Em- 605. (d) UV spectroscopy of Gd_2O_3 NCs and native medium molecular weight Chitosan.

5.3.2 Size and phase analysis

Figure 5.2 (a, b) shows the HRTEM image of ultrasmall Gd_2O_3 NCs. The histogram plot of obtained images revealed the formation of uniform-size Gd_2O_3 NCs with an average

diameter of 1.79 nm. This ultrasmall size of synthesized Gd_2O_3 NCs lies in the range of the reported optimal diameter (1–2.5 nm) for the maximum r_1 relaxivity and, therefore, can be used as an advanced T_1 MR imaging. [278] Furthermore, phase purity and crystallinity of Gd_2O_3NCs were examined via XRD analysis (Figure 5.2 (c)). The XRD pattern of Chitosan capped Gd_2O_3 NCs did not exhibit any characteristic peak of gadolinium oxide but displayed only one broad halo peak, which clearly indicated the amorphous nature of Gd_2O_3 NCs, originating due to the presence of ultrasmall nanoclusters. [248,446] Both HRTEM and XRD data supported the formation of ultrasmall Gd_2O_3 NCs.

5.3.3 Surface and infrared spectroscopy

The collaborated Fourier transform infrared spectroscopy (FTIR) and X-ray photoelectron spectroscopy (XPS) data analysis can provide insight into the chemical composition, oxidation state, and the interaction responsible for Gd_2O_3 NCs stabilization and associated fluorescence phenomena. XPS analysis found the characteristic peaks corresponding to Gd 4d (140.8 eV, 142.8 eV, 147.5 eV), C 1s (285.9 eV, 284.4 eV,287.5 eV), O 1s (530 .8 eV, 532.3 eV, 535.15 eV) (Figure 5.3), The binding energy was calibrated by centering the deconvoluted C 1s peak at 284.4 eV. The Gd 4d5/2 peak located at 140.8 eV and Gd 4d peak located at 142.9 eV indicating the existence of Gd^{3+}, whereas peak at 147.5 eV indicate the lowest s-CK distortions of the XPS line-shapes in the Gd 4d core-level spectrum. [448–451] O 1s peak located at 532.5 eV was correspond to C=O and C-OH functional group [452] and observed peak at 531.1 eV are harmonize with previously published Gd_2O_3 NPs synthesis report, [449] these peaks provide the evidence for the presence of oxygen containing groups and complexation Gd.

(a) **(b)**

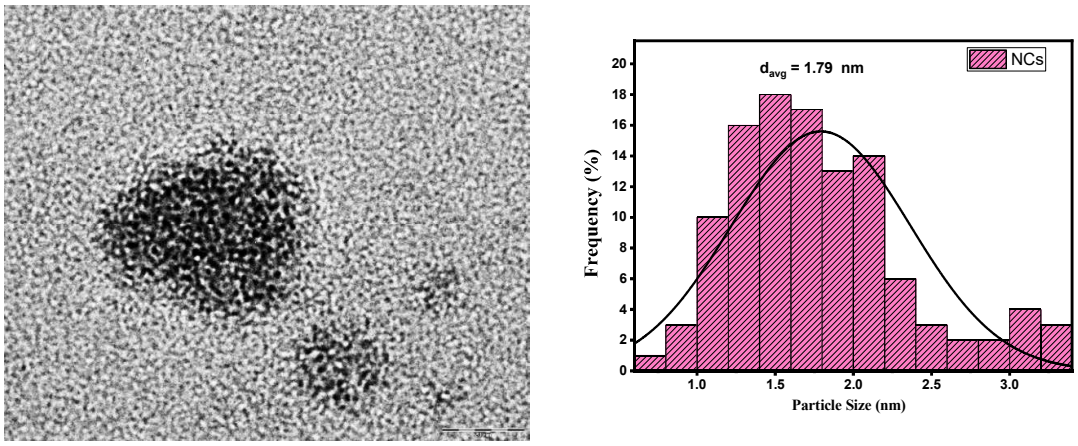

(c)

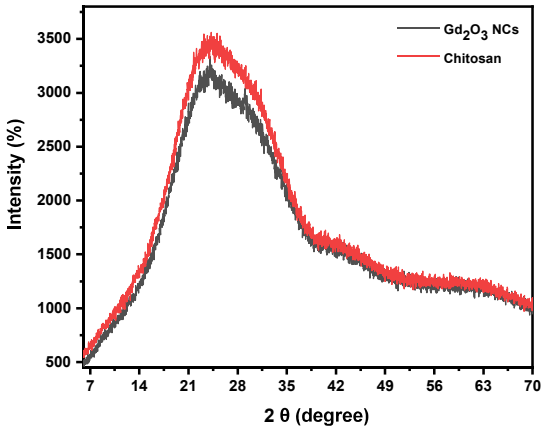

Figure 5.2: (a) Transmission Electron microscopy (TEM) image of prepared for Gd_2O_3 NCs, (b) Size distribution histogram for Gd_2O_3 NCs (sample size ~100), (c) XRD analysis of Gd_2O_3 NCs and native Chitosan polymer.

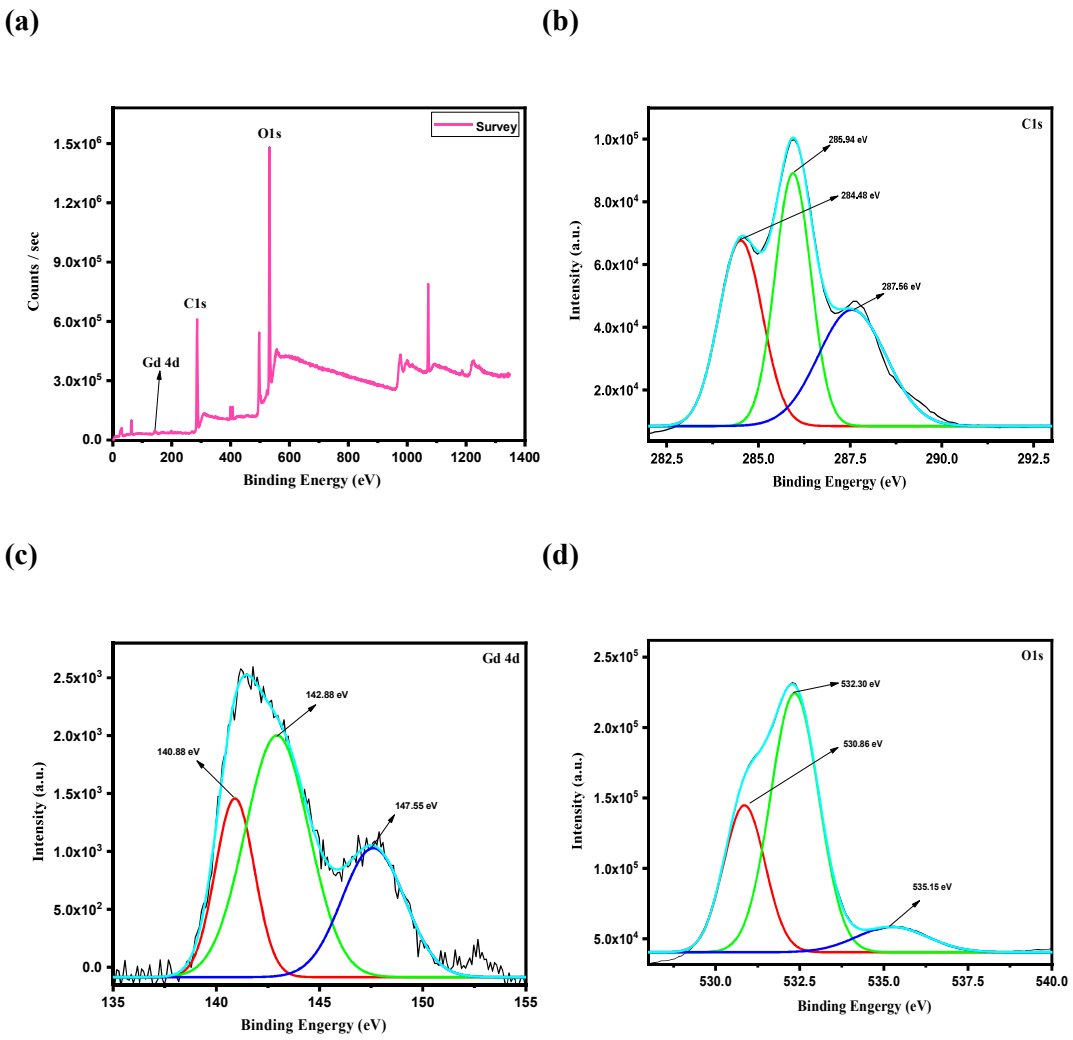

Figure 5.3: The XPS analysis of prepared Gd_2O_3 NCs. (a) The survey graph showing the presence of carbon, oxygen, and gadolinium in the sample, (b) a detailed analysis of C1s spectra showing a strong peak at 285.9 eV corresponding to carbonyl groups (C=O) and a small peak at 287.5 eV and 284.48 due to the Sp^3, Sp^2 hybridization respectively, (b) XPS analysis for Gd4d FTIR orbital, (d) XPS analysis for O1s orbital.

As seen in Figure 5.4 (a), the FTIR spectra of chitosan clearly show the vibration bands at wavelength 3279 cm^{-1} due to the presence of the O–H functional group; a peak at 2880 cm^{-1} corresponding to the C–H stretching; 1558 cm^{-1}, 1402 cm^{-1} peaks indicating the presence of amide group I, and II; 1002 cm^{-1} peak in correlation with the change of symmetry methyl.

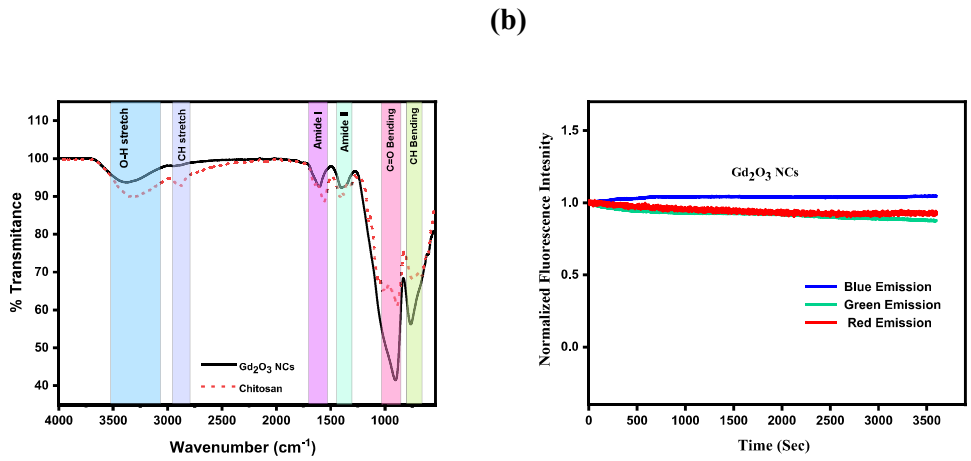

Figure 5.4: (a) FTIR spectrum analysis for prepared Gd_2O_3 NCs and native Chitosan polymer, (b) Normalized photostability study for Gd_2O_3 NCs emission at blue (Ex. 365), green (Ex. 465) and red (Ex. 550).

The band at 875 cm^{-1} can be attributed to the stretching of the C = S group 1151 cm^{-1} and 755 cm^{-1} peaks closely related to the structure of the saccharide (as repeating units of chitosan). [232,453] The chitosan, a chelating compound comprising two hydroxyl functional group of (OH) molecules and one amino functional group (NH_2) molecule can bind metal ions. When chitosan is present on gadolinium metal, the Gd_2O_3 NCs band shifts slightly to the right. This shift may be due to the interaction between protonation of the chitosan polymer with the adsorption of gadolinium on the active site. All hydroxyl (3279→3380), amine (N–H) stretching (1558→1608), C–H stretching (755→759), aldehyde (C=O) (1002→906) and aromatic ring peaks of Gd_2O_3 NCs were slightly shifted to the right side in comparison with the chitosan. This shift is due to degradation and crosslinking of the chitosan biopolymer that might have occurred after nanocluster formation. [454]

5.3.4 Stability of Gd_2O_3 nanoclusters

The stability of Gd_2O_3 NCs in terms of fluorescence intensity retention in the imaging application is the performance indicator. As we are aware, contrast agents are often endured through continuous light source exposure, which results in temporary or permanent loss of fluorescence. Besides, prolonged storage of NCs can also diminish fluorescence properties due to unwanted agglomeration resulting in bigger size particles due to several factors such as, Ostwald ripening, degradation of capping agent over time and change in electrostatic interactions. Also, for real-time application, ideal NCs properties could withstand a physiological pH range and tolerate ionic strength. Therefore, to confirm Gd_2O_3 NCs candidature for real-time imaging, we observed its shelf life, photostability, pH stability, ionic strength, and solvometric effect. The obtained result indicates that prepared Gd_2O_3 NCs retained their fluorescence (20% loss) for more than a year in both solution and powder phases. Additionally, Gd_2O_3 NCs demonstrated excellent photostability (60 minutes) (Figure 5.4 (b)), wide-range pH stability (5.8 to 11), good ionic tolerability (up to 1000 mM), and stability in different solvents such as DMSO, cyclohexane, ethanol, acetone, and methanol at excitation of 465 nm (Figure 5.5) and at the excitation of 365 nm. (Appendix Figure B1)

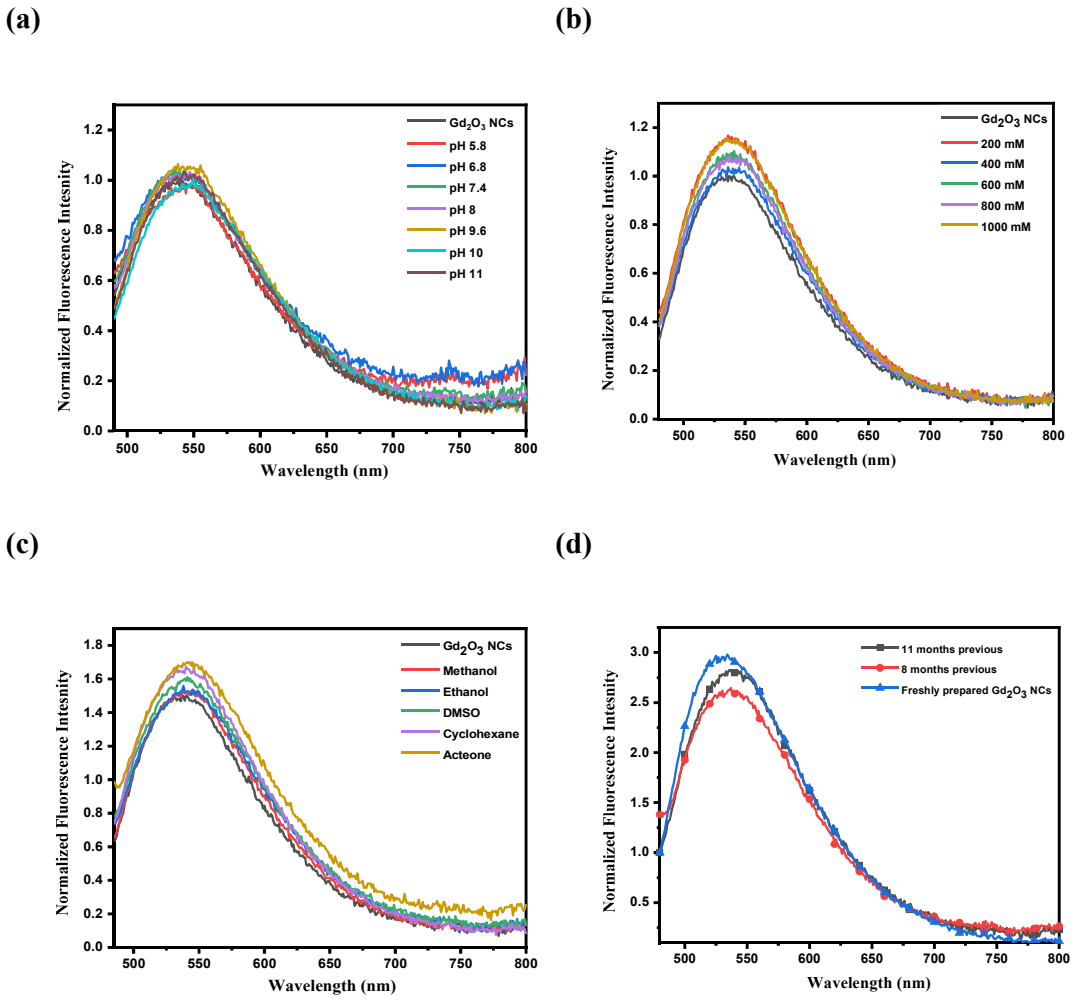

Figure 5.5: (a) pH. dependent normalized fluorescence emission spectra at different pH. (5.8-11) at λ_{Ex} 465 nm, (b) Normalized fluorescence emission spectra for Gd_2O_3 NCs after addition of various concentrations of freshly prepared NaCl solution at λ_{Ex} 465, (c) Normalized fluorescence emission spectra of freshly prepared Gd_2O_3 NCs with different solvent at λ_{Ex} 465, (d) Normalized fluorescence emission spectra for freshly prepared Gd_2O_3 NCs, previous 8 months and nearly 11 months old λ_{Ex} 465.

5.3.5 Mechanism behind synthesis

In this study, chitosan was solubilized using a 1% acetic acid solution. The chitosan reacts with H^+ from the acid solution to produce protonized chitosan with NH^{3+} functional groups. The emergence of these functional groups into the chitosan backbone enhanced its

solubility in water. When gadolinium salt was added to the chitosan solution, gadolinium ions attached to chitosan macromolecules by electrostatic interactions because the electron-rich oxygen atoms of polar hydroxyl and ether group chitosan are likely to interact with electropositive gadolinium cations. [455] Furthermore, a reducing agent is required to provide the free electrons needed to reduce ions and form nanoparticles. In this study, ascorbic acid was utilized as the reducing agent. Gd_2O_3 NCs thus were formed by the reduction of gadolinium ions. The Gd_2O_3 NCs are stabilized by protonized chitosan to prevent agglomeration and to control the size of the final nanoclusters developed. As shown in Figure 5.1, the emission intensity of Gd^{+3} chitosan increases with the addition of ascorbic acid. This enhancement is also conducted with a blue shift from 445 nm to 450 nm. This enhancement in the intensity is due to the ionic interactions between the amino groups (-NH_2) of chitosan with the hydroxyl (-OH) functional group of ascorbic acid. [456] Hence, the complex Gd_2O_3 NCs become more soluble due to enhancement of the hydrophilic properties. According to Tian et al., the ascorbic acid contains different electrophilic groups hence, it contains four hydroxyl groups with different acidities allowing in consequence different acid-base reactions. Therefore, the acidic hydroxyl in position 3 of ascorbic acid is expected to react with the amino group of chitosan, inducing the formation of ammonium ions. Thus, ammonium ions increase the solubility of the complex and thereby cause the enhancement of the emission intensity.[457]

5.4 Application of Gd_2O_3 Nanoclusters

5.4.1 Biocompatibility

Biocompatibility assessment of NPs prior to biological application is crucial to ensure they do not trigger harmful immune responses or toxicity when interacting with living organisms. This evaluation is vital for applications like bioimaging and nanomedicine, as

it enables safe and effective integration into biological systems, minimizing adverse effects and promoting desired outcomes. [458]

5.4.2 *In-vitro* cytocompatibility (MTT assay)

The cytocompatibility assay is a critical and primary need for the real-time delivery of any substance. MTT assay was used to investigate the effect of different concentrations of Gd_2O_3 NCs on the cell proliferation and viability of U-87 MG cells (Figure 5.6 (a)). The obtained results showed that developed clusters did not generate any toxicity and structural deformities in the treated cells even after higher concentrations (1/0 ratio of stock concentration (5.9 mg/ml)). Finally, the results show that the nanoclusters generated are extremely biocompatible and could be used in biological applications. [444]

5.4.3 Hemocompatibility assay

Blood compatibility analysis is a crucial and foremost step before administering any nanoprobe in real-time application. The haemolytic assay was used to determine the safety of the Gd_2O_3 NCs in the bloodstream (Figure 5.6 (b)). The percent hemolysis of DI water, Saline, and Gd_2O_3 NCs was 100 ± 6.83%, 2.98± 0.64%, and 3.25 ± 0.18%, respectively. The results validated that Gd_2O_3 NCs did not induce toxicity in blood cells; that is, they were hemocompatible at the concentrations employed for the bioimaging and cell viability assays (5.9 mg/ml), which is consistent with earlier research. Thus, the blood compatibility assay substantiates the potential of Gd_2O_3 NCs for in-vivo applications. [224,459]

(a) **(b)**

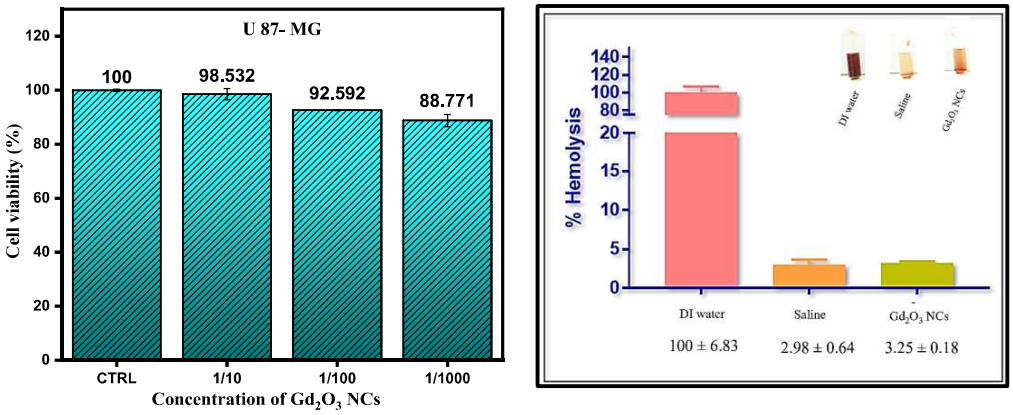

Figure 5.6: (a) MTT analysis of Cell Proliferation on U-87 MG (Glioma Brain Cell), (b) Hemocompatibility test for nanoclusters with positive and negative control with Di water Saline, respectively.

5.4.4 *In-vivo* Cytocompatibility test

The control group in this study received a normal saline solution and showed no pathological abnormalities in the brain, lungs, liver, kidneys, or spleen. Moreover, at the 3 hrs., 7 days, and 28 days' time intervals, no degenerative abnormalities were identified in these organs for the Gd_2O_3 NCs-treated group (Figure 5.7). These findings imply that the injection of Gd_2O_3 NCs was deemed safe and non-toxic for *in-vivo* use. [234,460]

A careful evaluation of the rat's behaviour before and after dosing with the Gd_2O_3 NCs revealed no signs of abnormalities and peculiarity. Animal behaviour was typical, as was mobility within the cage and food consumption. Furthermore, we found no evidence of trauma or fatality. The body weights of the rats before and after dosage are shown below.

Table 5.1: Rats' body weight before and after Gd_2O_3 NCs administration

Group	Before administration (gm)	2nd day (gm)	7th day (gm)	28th days (gm)
Control	190	192	195	198
	195	193	190	196
	201	199	202	205
Gd_2O_3NCs treated	205	203	207	201
	195	196	192	198
	204	202	197	206

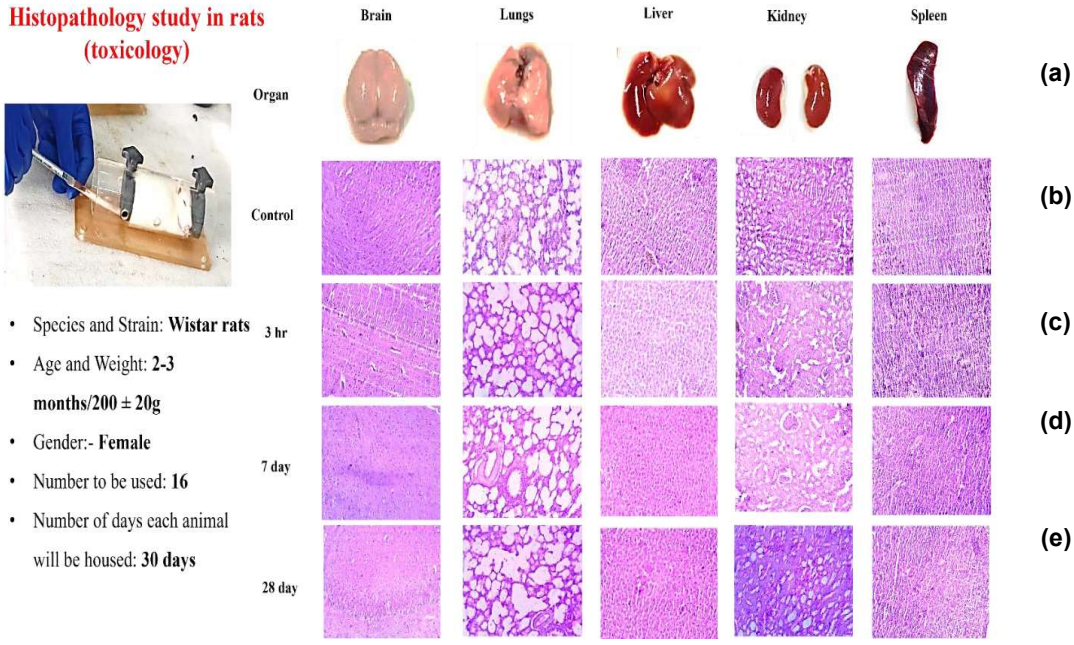

Figure 5.7: Histopathological appearance in H & E-stained rat liver sections of all groups; (a) Real image of organ taken after 28 days of injecting nanoclusters, (b) Normal tissue without injecting nanocluster (control group); (c) Tissue appearance (3 hrs) after injecting nanocluster through tail vein injection (d) Tissue appearance (7 days) after injecting nanocluster through tail vein injection, (e) Tissue appearance (28 days) after injecting nanocluster through tail vein injection. Bar: 10 μm

5.4.5 In-vitro cell imaging

Negligible cytotoxicity, and water solubility, along with tunable fluorescence intensity and high quantum yield, make Gd_2O_3 NCs a potential candidate for cell imaging and labeling purposes. In this study, we took human glioma cells (U-87 MG) to visualize and quantify Gd_2O_3 NCs cytoplasmic accumulation under a confocal microscope. Acquired images at same scale of Gd_2O_3 incubated cells demonstrated bright red, green, and blue emission, whereas control 1 (Chitosan protein) (Appendix Figure B 2) and control 2 (Without salt) displayed weak emission in blue channels due to the intrinsic fluorescence property of diluted chitosan. [461] The fluorescence signal was observed to be concentrated in the cytoplasm rather than the nucleus. This result suggests that prepared clusters can be effectively utilized to stain living cells as well as monitor them in real time. [446,447] (Figure 5.8)

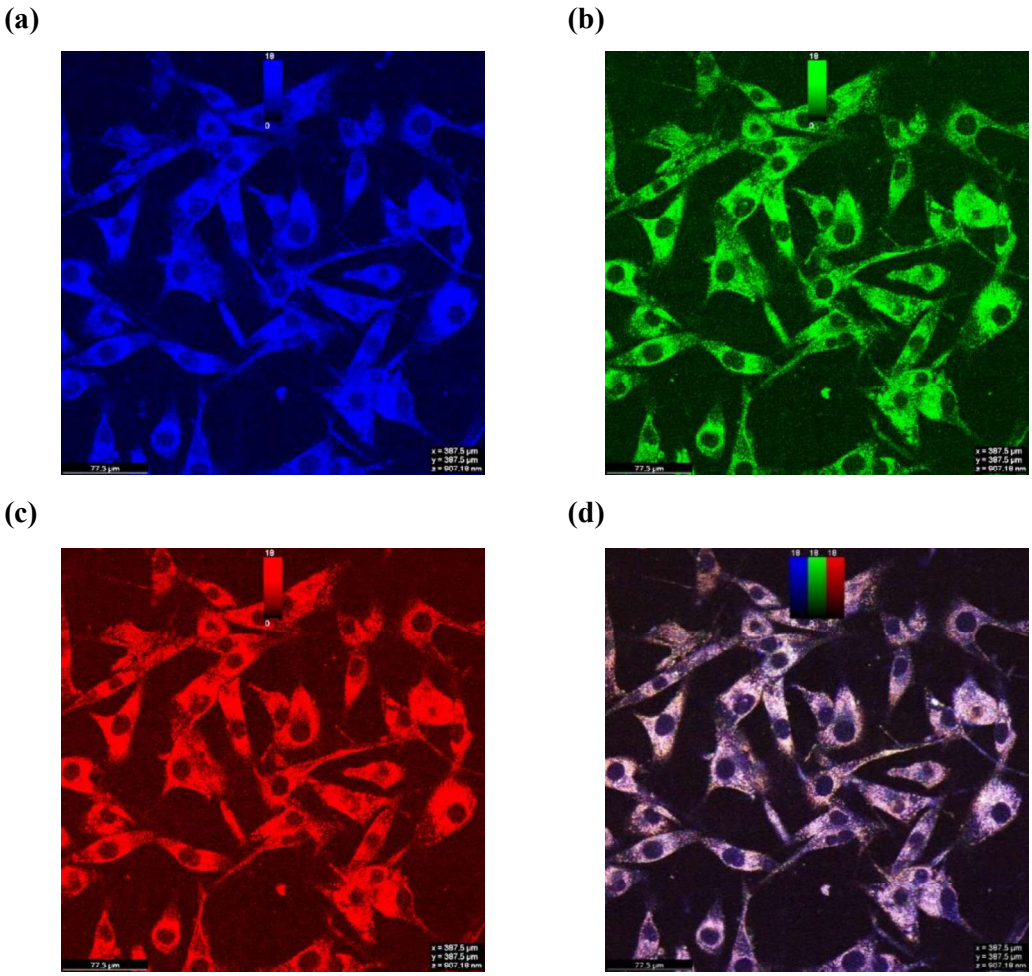

Figure 5.8: Multifluorescent confocal imaging of U 87-MG cells treated with Gd_2O_3 NCs (5.9 mg/ml of stock solution) at different excitation of (a) Ex. /Em-366 nm/blue, (b) Ex. /Em-472 nm/green, (c) Ex. /Em-472 nm/red, (d) merged image.

5.4.6 Z stacking (focus stacking) Confocal Analysis

Confocal microscopy sharpens the images by viewing light from a single plane of focus. This enables the collection of numerous focus planes in a three-dimensional data set known as a Z-stack. The Z-stack imaging is a series of images taken at predetermined intervals between the first and last planes focusing on surrounding cells. These photos are integrated into a brief "Real-time" video, which allows users to study the Cells at any plane of focus

without using a microscope. The Z-stacking is a digital image processing approach that combines all photos acquired at various focal lengths to produce a composite image with a higher depth of field (i.e., the thickness of the plane of focus) than any of the individual source images.

Confocal Z-stack analysis was used to perform the mean fluorescence intensity of prepared Gd_2O_3 NCs at various places inside the cell. This investigation entailed inspecting various slices of the complete cell to determine the nanocluster's distribution inside the cell. The cell was cut into ten slices, each of which contained Gd_2O_3 NCs. 0 µm to 24 µm were shortened as the lowest and higher parts of the cell surface, and Z-stack confocal cell pictures (10 slices) were taken for incubation with prepared nanoclusters. The Mean fluorescence intensity was computed and analyzed for each slice of the cell surface using an excitation wavelength of λ_{ex} 366 nm and a corresponding emission wavelength of λ_{em} 477 nm. (Figure 5.9) The detailed study of the mean fluorescent intensity graph revealed that the highest intensity (100%) was seen at a distance of 6 µm above the cell's lower surface, indicating that the central section of the cell surface exhibits the most fluorescence. The lowest intensity (44.27%) was detected at 22 µm, which represents the cell's second-most surface, implying that the second-most layer of the cell includes a lesser concentration of nanoclusters. Figure B1 shows a multifluorescent confocal image of U 87-MG cells treated with just Chitosan polymer in blue, green, and red. As a result, the mean fluorescence intensity patterns for blue emitting Gd_2O_3 NCs. are as follows: (a) = 62.63%, (b) = 84.02%, (c) = 99.16%, (d) = 100%, (e) = 97.17%, (f) = 78.12%, (g) = 72.84%, (h) = 68.21%, (i) = 51.92%, (j) = 51.34%, (k) = 47.55%, (l) = 44.27%, (m) = 47.05%. (Appendix Figure B3)

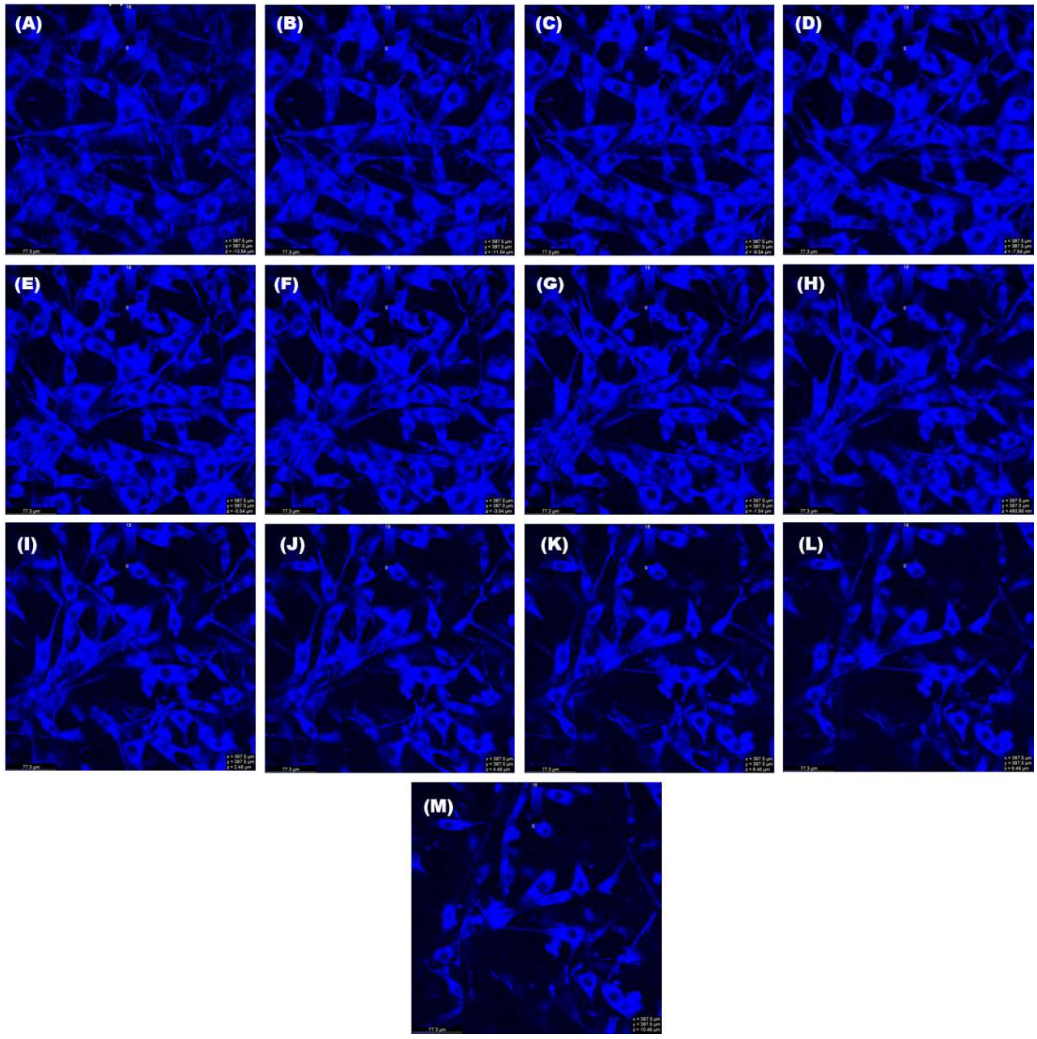

Figure 5.9: Z stack confocal images and Mean Luminescence Intensity in U 87-MG cells for Gd_2O_3 NCs. [Ex. 366 nm, Em. Blue (477 nm)] (a) = 0 µm, (b) = 2µm, (c) = 4µm, (d) = 6µm, (e) = 8µm, (f) = 10µm, (g) = 12µm, (h) = 14 µm, (i) = 16 µm, (j) = 18 µm, (k) = 20 µm, (l) = 22 µm, (m) = 24 µm.

In similar way, the mean fluorescence intensity calculated at λ_{ex} 472 nm and a corresponding emission wavelength of λ_{em} 541 nm. (Figure 5.10) The detailed study of the mean fluorescent intensity graph revealed that the highest intensity (100%) was seen at a distance of 6 µm above the cell's lower surface, indicating that the central section of the cell surface exhibits the most fluorescence in a similar way of blue excitation but the lowest

intensity (16.76%) was detected at 20 µm, which represents the cell's third uppermost surface, implying that the third most layer of the cell includes a lesser concentration of nanoclusters. As a result, the mean fluorescence intensity patterns for green-emitting Gd_2O_3 NCs. are as follows: (a) = 24.69%, (b) = 58.95%, (c) = 97.85%, (d) = 100%, (e) = 90.21%, (f) = 83.28%, (g) = 72.41%, (h) = 46.74%, (i) = 26.94%, (j) = 22.23%, (k) = 16.76%, (l) = 26.44%, (m) = 18.29%. (Appendix Figure B4)

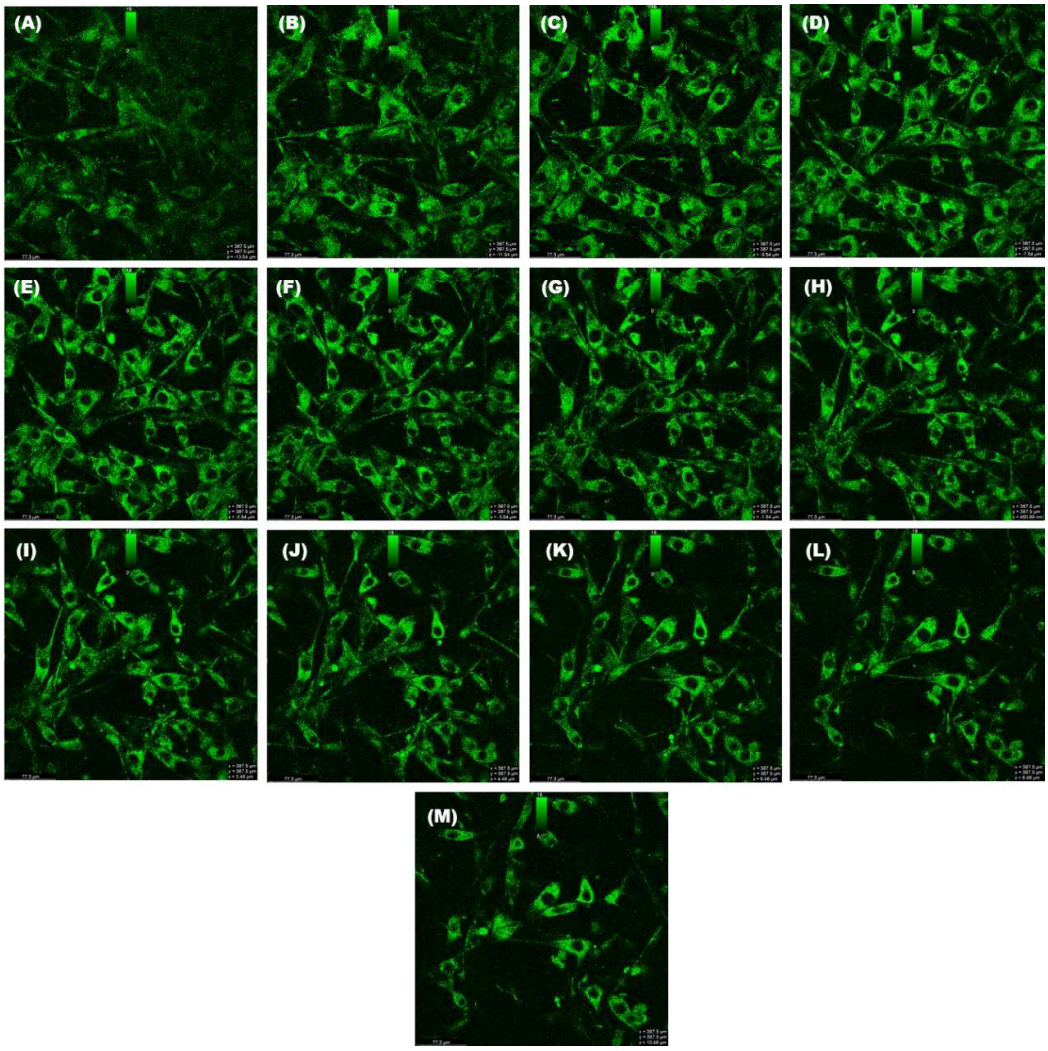

Figure 5.10: Z stack confocal images and Mean Luminescence Intensity in U 87-MG cells for Gd_2O_3 NCs. [Ex. 472 nm, Em. Green (541 nm)] (a) = 0 µm, (b) = 2µm, (c) = 4µm, (d) = 6µm, (e) = 8µm, (f) = 10µm, (g) = 12µm, (h) = 14 µm, (i) = 16 µm, (j) = 18 µm, (k) = 20 µm, (l) = 22 µm, (m) = 24 µm.

But in Z stacking in red, the mean fluorescence intensity calculated at λ_{ex} 472 nm and a corresponding emission wavelength of λ_{em} 636 nm. (Figure 5.11) Unlike blue and green emissions, the mean fluorescent intensity graph revealed that the highest intensity (100%) was seen at a distance of 8 µm above the cell's lower surface, indicating that the central section of the cell surface exhibits the most fluorescence but the lowest intensity (18.72%) was detected at 24 µm, which represents the cell's uppermost surface, implying that the uppermost layer of the cell includes a lesser concentration of nanoclusters. As a result, the mean fluorescence intensity patterns for red-emitting Gd_2O_3 NCs. are as follows: (a) = 30.27%, (b) = 55.22%, (c) = 95.42%, (d) = 96.89%, (e) = 100%, (f) = 94.82%, (g) = 76.90%, (h) = 57.43%, (i) = 33.43%, (j) = 24.34%, (k) = 23.96%, (l) = 27.51%, (m) = 18.72%. (Appendix Figure B5)

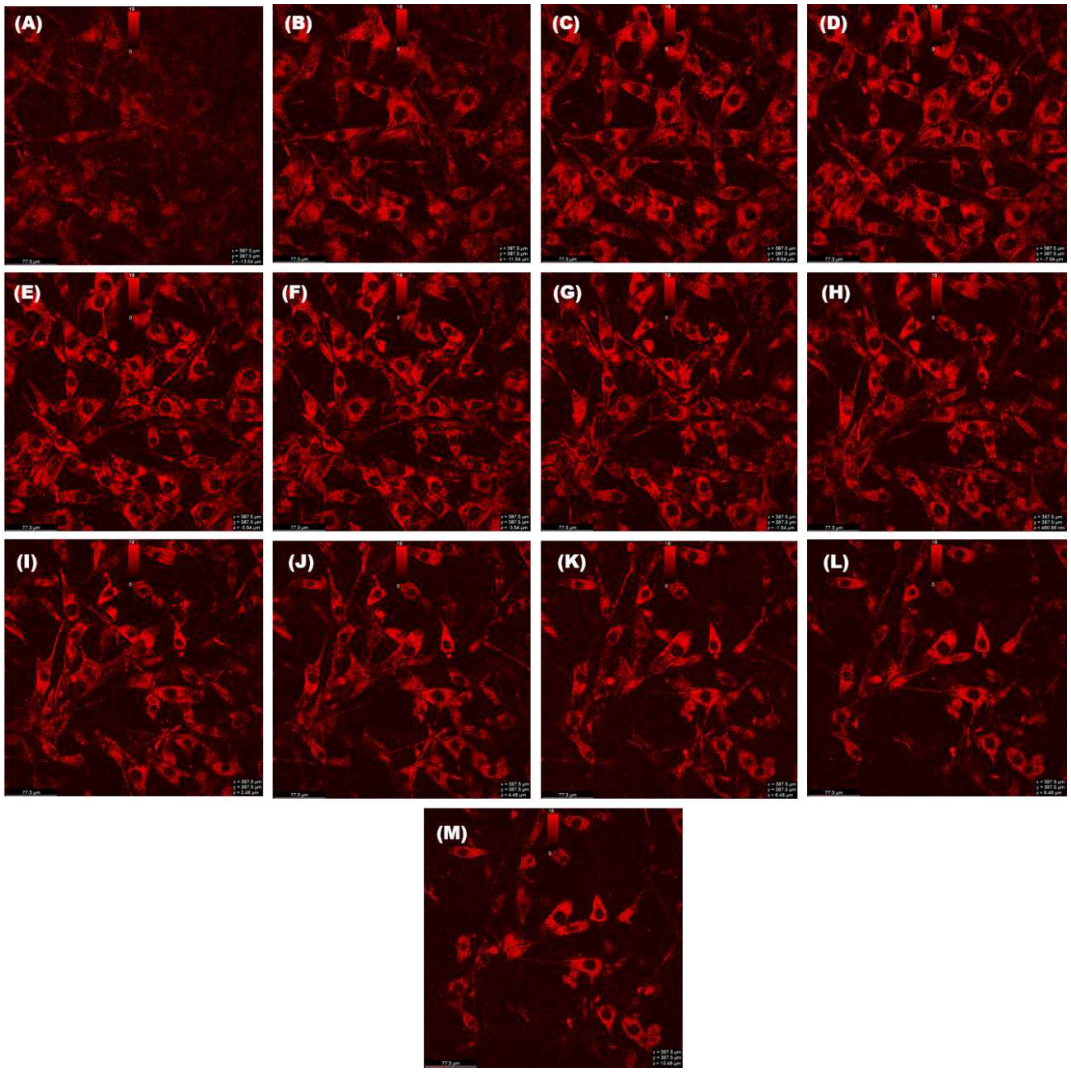

Figure 5.11: Z stack confocal images and Mean Luminescence Intensity in U 87-MG cells for Gd_2O_3 NCs. [Ex. 472 nm, Em. Red (636 nm)] (a) = 0 µm, (b) = 2µm, (c) = 4µm, (d) = 6µm, (e) = 8µm, (f) = 10µm, (g) = 12µm, (h) = 14 µm, (i) = 16 µm, (j) = 18 µm, (k) = 20 µm, (l) = 22 µm, (m) = 24 µm.

5.4.7 *In-vivo* imaging system (IVIS imaging)

To investigate the biodistribution and renal clearance and imaging capability in physiological condition of Gd_2O_3 NCs were investigated using In-vivo imaging system.

The intravenous injection of 200 µl of Gd_2O_3 NCs (5.9 mg/ml stock solution), through tail vein of the mice were performed and the fluorescence intensity was monitor in different time intervals (0 min, 15 min, 30 min, 1 hr, 3 hrs. 6 hrs) emitted by live cell of mice using IVIS imaging systems. Following a series of time intervals subsequent to injection, the distribution of Gd_2O_3 NCs was visualized within the vital organs of the mice (liver, lungs and kidney).

In the group treated with Gd_2O_3 NCs, a significant proportion of the administered nanoclusters remained in the bloodstream following intravenous injection. This can be attributed to the stable interaction between Gd_2O_3 NCs. After a duration of 15 min to 30 min, the Gd_2O_3 NCs were mostly localized in the vital organs of mice, after 3 hrs. of injecting Gd_2O_3 NCs. The IVIS imaging showed maximum accumulation in bladder region which play a crucial role in nanoclusters to disposal. This study provides validation for the *in-vivo* imaging efficiency Gd_2O_3 NCs and confirming their distribution and clearance., this phenomenon demonstrates its inherent potential as a valuable instrument for the purpose of non-invasive visualization and tracking.

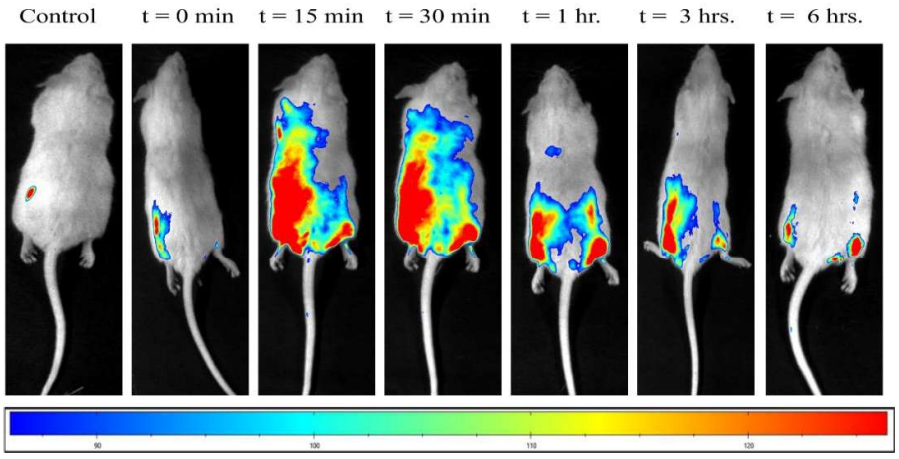

Figure 5.12: Live animal fluorescent images of Gd_2O_3 NCs treated mice in different time intervals.

5.4.8 Relaxivities Measurement

The r_1 was estimated to be 7.9 from the slopes in the plot of $1/T_1$ as a function of different concentrations of Gd_2O_3 (Figure 5.13). The measured relaxivity is also provided in the table 5.2, along with commercially available gadolinium contrast agents. The value of r_1 is almost two times larger than those commercially available Gd (III)-chelates. [247,462]

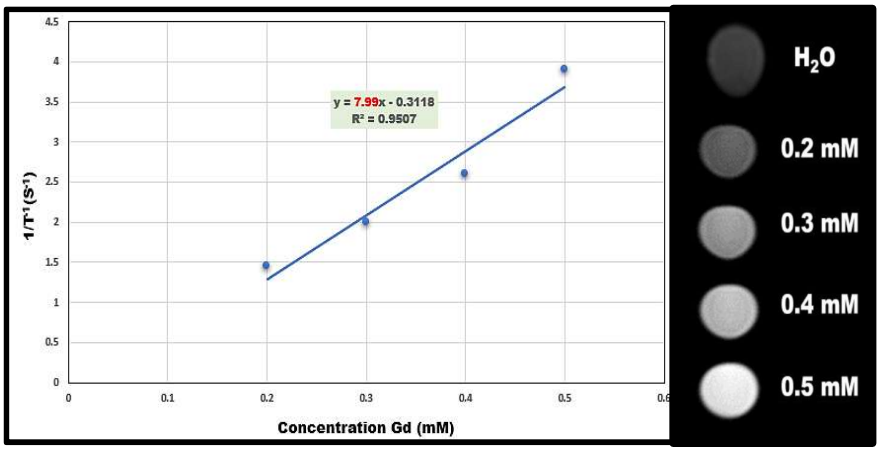

Figure 5.13: T1- weighted MR images of Gd_2O_3 NCs with various concentrations (equivalent Gd concentration: 0.2, 0.3, 0.4, 0.5, 1, 1.5 mM), and linear correlation between longitudinal relaxivity {r_1 (ms)} with equivalent Gd concentration of Gd_2O_3 NCs.

Table 5.2: Comparative table of Gd_2O_3 nanoclusters along with commercially available contrast agents.

Contrast agent	Magnetization (Tesla)	Relativity ($mM^{-1}s^{-1}$)
Magnevist ®	3.0T	3.7
MultiHance®	3.0T	5.5
Omniscan®	3.0T	4.0
Dotarem®	3.0T	3.5
ProHance®	3.0T	3.7
Gadavist®	3.0T	5.0
Eovist®	3.0T	6.2
Gd_2O_3 NCs (This Work)	**3.0T**	**7.9**